

Article

# On-Line Feedback Control of Sliding Friction of Metals Lubricated by Adsorbed Boundary SDS Films

Chenxu Liu <sup>1</sup>, Xiaosong Li <sup>1</sup>, Xinxin Li <sup>1</sup>, Weizi Li <sup>2</sup>, Yu Tian <sup>1</sup> and Yonggang Meng <sup>1,\*</sup>

<sup>1</sup> State Key Laboratory of Tribology, Tsinghua University, Beijing 100084, China; lcx@mail.tsinghua.edu.cn (C.L.); lixs18@mails.tsinghua.edu.cn (X.L.); lixinxin17@mails.tsinghua.edu.cn (X.L.); tianyu@mails.tsinghua.edu.cn (Y.T.)

<sup>2</sup> Shell (Shanghai) Technology Limited, Shanghai 201210, China; wayne.li@shell.com

\* Correspondence: mengyg@tsinghua.edu.cn; Tel.: +86-010-62773867

**Abstract:** The on-line feedback control of sliding friction of metallic tribopairs lubricated by adsorbed sodium dodecyl sulfate (SDS) films was demonstrated on a customized tribosystem, in which the external electric field applied on the tribopair was modulated in feedback according to the electrical contact resistance signal. When a positive voltage was applied, the adsorption of SDS anions on the surface of tribopair was enhanced so that the boundary film was stable. When the contact resistance increased to a pre-set threshold (e.g., 6~10  $\Omega$ ), which indicated the formation of a relatively complete boundary film, the external voltage was switched off for saving energy. For an aqueous solution with 160 mM SDS as the lubricant, the coefficient of friction (COF) was decreased by 24% for the 316 L plate/304 steel ball under 804 MPa by modulating the applied potential of +3.5 V. For the propylene carbonate lubricant with 5 mM SDS, the COF was decreased by 39% for the Cu plate/304 steel ball under 499 MPa and 54% for the Cu plate/bearing steel ball under 520 MPa by modulating the applied potential of +20 V. This novel approach could be effective to keep good boundary lubrication of machine components under variable work conditions by on-line sensing and actuation.

**Keywords:** tribotronics; boundary lubrication; electric field; contact resistance; feedback control



**Citation:** Liu, C.; Li, X.; Li, X.; Li, W.; Tian, Y.; Meng, Y. On-Line Feedback Control of Sliding Friction of Metals Lubricated by Adsorbed Boundary SDS Films. *Lubricants* **2022**, *10*, 148. <https://doi.org/10.3390/lubricants10070148>

Received: 12 May 2022

Accepted: 29 June 2022

Published: 11 July 2022

**Publisher's Note:** MDPI stays neutral with regard to jurisdictional claims in published maps and institutional affiliations.



**Copyright:** © 2022 by the authors. Licensee MDPI, Basel, Switzerland. This article is an open access article distributed under the terms and conditions of the Creative Commons Attribution (CC BY) license (<https://creativecommons.org/licenses/by/4.0/>).

## 1. Introduction

Engineering frictional interfaces often operate in a complex environment and under varying lubrication conditions [1]. Although most modern machine components are so designed that their frictional interfaces are under fluid film lubrication in typical working conditions, frequent cold start-up, shutdown, as well as overloading and/or overheating, of machine systems during service make the fluid film lubrication state non-maintainable constantly, and mixed lubrication and boundary lubrication are inevitable. As lubrication shifts from fluid film lubrication, friction and wear of machine components increases usually substantially, resulting in not only higher energy loss but also occasional mechanical failures. To prevent poor lubrication during the operation of machine systems without altering the design and materials of machine components, the approach of active tribology or tribotronics is a promising way for current mechanical systems in the industry [2]. Especially with the development of electric vehicles and hybrid vehicles [3], there will be more frequent stop-starts than for conventional vehicles, potentially leading to higher levels of wear. How to actively control boundary lubrication is a very important subject among the current tribological challenges [4].

Almost all of the present tribological contacts are non-adjustable on-line, or passive in other words, the geometry, material, and lubricant are all pre-determined in the stages of design and manufacturing. These kinds of systems are sensitive to any increase in severity of operating conditions [2], whose performance cannot be tuned on-line. The design of the active control method for multiscale friction, including the use of magnetic and electric fields external to the contact [5] has been extensively studied. In around 1950,

Bowden and Young introduced the potentiostatic technique of electrochemistry to the field of tribology [6]. In 1969, Bockris et al. observed that the coefficient of friction (COF) between two solids in electrolytes varied parabolically with potential [7]. In 1989, Wang and Tung used electrochemical methods for understanding the reactions between several zinc organodithiophosphate (ZDP) anti-wear additives and cast iron surfaces [8]. They developed an in-situ electro-charging technique to enhance the effectiveness of ZDP additives as anti-wear and friction-reducing agents in typical engine oils [9]. In 1994, Spikes et al. tested the influence of electrochemical potentials on the tribological behaviors of iron/iron and iron oxide/alumina oxide rubbing contacts in aqueous salt solutions and thought that electrochemical potentials could influence friction coefficient by modifying electrochemical double layer effects and controlling the surface chemistry, and then the shear strengths of the films present on the rubbing surfaces [10]. Since 1998, Meng et al. focused on studies on the potential-controlled friction for aqueous and non-aqueous solutions with surfactants, anti-wear additives, or nanoparticles [11–14]. Further, it has been found that electrostatic interaction plays an important role in the potential-controlled friction phenomena. Meanwhile, on-line control of friction had struggled with the understandings of the electrical response behavior of base lubricant or lubricant additives. In 2001, active control of COF of  $\text{Al}_2\text{O}_3/\text{Cu}$  rubbing couples in zinc stearate water suspension was demonstrated in the pre-assigned goal of either a step-rise change or a sinusoidal variation [15]. The discrepancy of the COF under control was successfully suppressed by less than 3% of the goal values, although the response of the system was not fast. In 2020, Gatti et al. [16] built a tribological system to control itself and maintain given friction values as a function of time by applying a single electrical anodic pulse when two metallic friction partners are lubricated with ionic liquid mixtures. These methods attract increasing attention, as they address one of the present-day's grand challenges: achieving in situ control of friction without removing and replacing lubricants [5]. However, potential-controlled friction is still a laboratory art and has not been applied in the industry yet. The technological obstacles to practical applications are speculated as below.

To achieve in-situ feedback control of lubrication state, an effective and reliable on-line technique to detect and identify the shifting of lubrication regimes is necessary. Unfortunately, it is difficult to observe and monitor the lubrication state directly, owing to the hindered contacting and moving interfaces in machine systems. Some available experimental methods on solid-liquid interfaces, such as quartz crystal microbalances, have been used to characterize the adsorption behavior of molecules or ions on solids. However, such methods are generally off-line characterization, and thus limited to scientific studies in the laboratory only. Surface morphology observation and chemical structure measurement can be carried out on specific instruments to analyze the post-friction surfaces, but do not enable on-line real time detection. In the laboratory, frictional force, or COF, is measurable on a tribometer. However, it is not always possible to measure frictional force and load acting on individual interfaces in many industrial applications, due to the complex structure and movements in real machinery.

Among many physical and chemical phenomena relating to friction and lubrication, electrical contact resistance (ECR) [17,18] and acoustic emission (AE) [19] are considered to be of their advantages for the testing of mixed or boundary lubrication. Since the 1940s, ECR has been used to study the real contact area between conductive solids and solids during static and sliding processes [20–22]. It provided an important experimental reference for theoretical research of tribology and contact mechanics. In general, ECRs are composed of constriction and film resistances, as functions of hardness, temperature, electrode force, and surface condition [23]. The former is the resistance caused by the current line contraction; the latter is caused by the contact surface being covered by some layers with poor electrical conductivity [24]. With the in-depth study of lubricant additive mechanism under boundary lubrication, ECR has been widely used to analyze the formation process of tribochemical reaction film on-line [25,26]. Previous investigations have indicated that ECR

can characterize the formation and failure of the adsorption film on the metallic surfaces of tribopairs.

In this study, we focus on the demonstration of a tribosystem with active sensing and actuation functions. By combining an ECR module, an external electric field module, and an active control software design, the COF of metallic tribopairs in aqueous or non-aqueous solutions with surfactants can be controlled in feedback during sliding. It is expected to provide a new pathway for on-line sensing and actuation technologies for tuning boundary lubrication according to variable working conditions.

## 2. Materials and Methods

Friction tests were conducted on a micro-tribometer (UMT-3, Bruker, Karlsruhe, Germany) at room temperature. The tests were carried out at a sliding speed of 8 mm/s over a 4 mm track. The reciprocating frequency was 1 Hz. Either a 304 steel ball (hardness of 4.7 GPa and Young's modulus of 174.1 GPa) or a bearing steel ball (hardness of 12.0 GPa and Young's modulus of 202.5 GPa) with a diameter of 6.35 mm was used as the upper friction pair. Either 316 L steel plate (size of  $20 \times 20 \times 3 \text{ mm}^3$ , hardness of 4.8 GPa and Young's modulus of 171.7 GPa) or pure Cu plate (size of  $20 \times 5 \times 3 \text{ mm}^3$ , hardness of 1.7 GPa and Young's modulus of 126.3 GPa) with a surface roughness  $R_a$  of  $\sim 10 \text{ nm}$  was used as the lower friction pair. The normal load applied to the ball-on-flat surface was 1 N or 3 N. According to the Hertzian contact model, the pressure was 804 MPa for 316 L steel plate vs. 304 steel ball under the load of 3 N, 499 MPa for Cu plate vs. 304 steel ball under 1 N, and 520 MPa for Cu plate vs. bearing steel ball under 1 N. Sodium dodecyl sulfate (SDS, 95%, Beijing Solarbio Science and Technology Co., Ltd., Beijing, China) dissolved in deionized  $\text{H}_2\text{O}$  with a resistivity of  $18.2 \text{ M}\Omega\cdot\text{cm}$  or propylene carbonate (PC, 99%, Shanghai Macklin Biochemical Co., Ltd., Shanghai, China) was used as the lubricant.

Contact resistance was measured using the Kelvin four-wire method with an auto ohmmeter (TH2512; Changzhou Tonghui Electronic Co., Ltd., Changzhou, China). The sampling frequency was set to be 1.7 Hz or 5.0 Hz. A direct current (DC) power supply was employed in the experiment to provide electric potential. The lower friction pair was used as the work electrode, and a Ti alloy plate ( $20 \times 10 \times 2 \text{ mm}^3$ ) as the counter electrode. Figure 1a presents the schematics of the experimental setup, which merges the tribometer, the DC power supply (two electrodes system), and the auto ohmmeter.

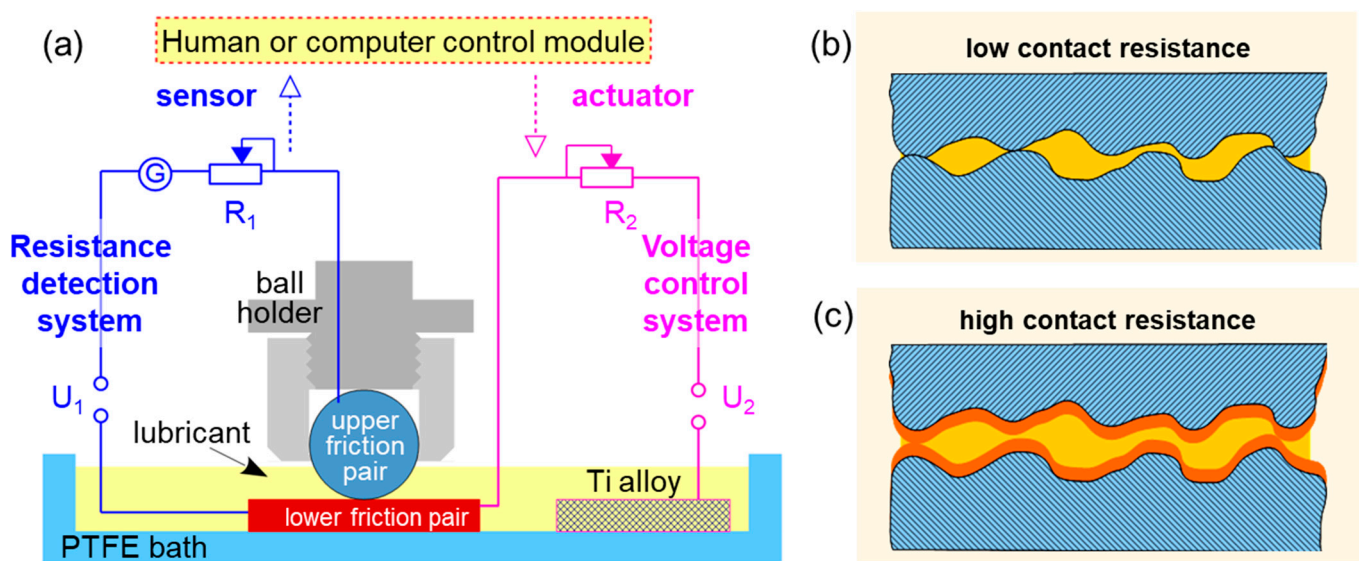


**Figure 1.** Schematic diagrams of (a) a tribometer combined with a DC power supply and an auto ohmmeter, metallic asperity contacts lubricated by (b) poor boundary lubrication film, and (c) good boundary lubrication film.

The design idea in this study is described as follows. Under poor boundary lubrication, the adsorption film composed of SDS surfactant in the contact area fails and metallic asperity contacts are formed. Hence, the COF is relatively high, and the contact resistance between the ball and plate is low. When a complete boundary lubrication film is formed, the COF becomes low, and the contact resistance gets higher. The schematic diagrams of the models under poor and good boundary lubrication are shown in Figure 1b,c, respectively.

This basic mechanism provides a possible way to dynamically modulate the applied potential by monitoring the contact resistance in real time. Therefore, we built a customized tribometer that can dynamically modulate the external electric field between the lower friction pair and a counter electrode (Ti alloy plate), based on the real time feedback of collected contact resistance between the friction pairs, as shown in Figure 2. The computer acquires the real time detected contact resistance signals via serial communication from the ohmmeter. If the contact resistance is smaller than a pre-set threshold, the computer sends a corresponding command to the DC power via serial communication to apply specified potential. If the detected contact resistance signal is higher than the pre-set threshold, the external electrical potential is switched off. By specifying the control frequency and threshold reasonably, this method can control the lubrication state on-line.

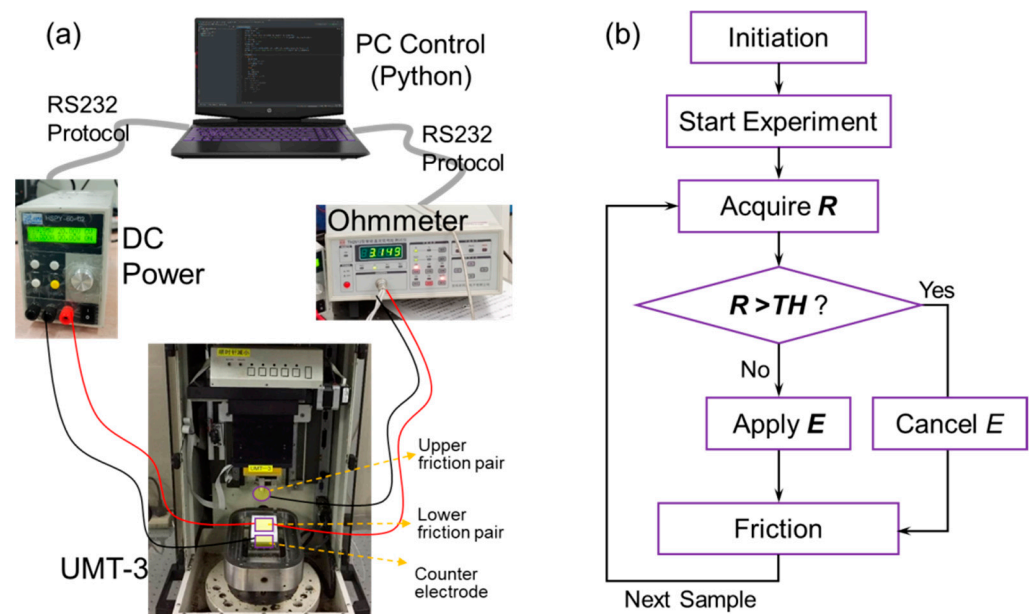


**Figure 2.** (a) The main modules composition and (b) the control logic block diagram of the feedback control system of the tribometer. In the diagram, the contact resistance, the threshold, and the electrical potential are denoted by  $R$ ,  $TH$ , and  $E$ , respectively.

After the friction tests, microstructure and elementary compositions of the wear tracks of the lower friction pairs were characterized by an optical microscope (Keyence, Japan) and a scanning electron microscope (SEM, Quanta 200 Environmental Scanning Electron Microscope, FEI, Eindhoven, Netherlands) combining with an energy-dispersive X-ray spectroscopy (EDX). Surface profiles of the wear tracks were measured on 3D optical profiling instruments (ZYGO NexView, Middlefield, CT, USA).

### 3. Results and Discussion

#### 3.1. Effect of External Electric Field on COF and Contact Resistance

By combining the contact resistance with COF, the SDS adsorption film formation and failure on the surface of stainless steel or Cu plate when rubbing against stainless steel or bearing steel ball were analyzed under different applied electrical fields.

Figure 3 shows the COF and contact resistance of 316 L stainless steel plate and 304 stainless steel ball verse time, under dry friction and lubricated by pure water as well

as 160 mM SDS aqueous solution. In the first 100 s, the friction pair was under dry friction with a high COF of  $1.04 \pm 0.07$  and a low contact resistance of  $3.6 \Omega$ . Then, around 0.25 mL of pure water was injected into the contact area. The COF decreased to  $0.37 \pm 0.04$ , and the contact resistance was stable at  $3.0 \Omega$ . For macroscale rough surface contacts, the load-carrying capacity of pure water is relatively poor. The addition of some kinds of long-chain organic molecules can improve boundary lubrication of aqueous solutions [27]. At 200 s, 20 mL of 160 mM SDS aqueous solution was added into the contact area. The COF decreased from  $0.37 \pm 0.04$  to  $0.23 \pm 0.01$ . The SDS surfactant shows a better lubrication effect, compared with  $H_2O$  molecules. At 300 s, a positive voltage of 3.5 V was applied, with the lower friction pair of 316 L stainless steel as the work electrode and an external Ti alloy plate as the counter electrode as shown in Figure 1a. The positive voltage represented that the work electrode was contacted with the positive pole of the power supply. The COF decreased to  $0.18 \pm 0.01$ , and the contact resistance obviously increased from  $3.3 \Omega$  to  $12.4 \Omega$ . The mechanism considered is that when the metal plate works as a positive pole, the surface concentration of SDS anions ( $DS^-$ ) becomes higher due to the field-assisted adsorption. When a negative potential of 3.5 V was applied on the surface of the lower friction pair, the COF increased to  $0.45 \pm 0.01$ , and the contact resistance decreased to around  $3.4 \Omega$ . The results indicated that a complete boundary lubrication film was formed on the surface of friction pairs in SDS solution under the positive potential of 3.5 V, and destructed owing to the desorption of SDS anions under the negative potential of 3.5 V. In the absence of external electric field, the COF decreased to  $0.31 \pm 0.01$ , and the contact resistance was about  $2.6 \Omega$ . The changes of the COF under different voltages in SDS solutions are consistent with the regularity reported by previous studies [11]. Meanwhile, the contact resistance result shows more detailed information on the formation and failure of the boundary film during the friction testing, which will be discussed in Section 3.3.

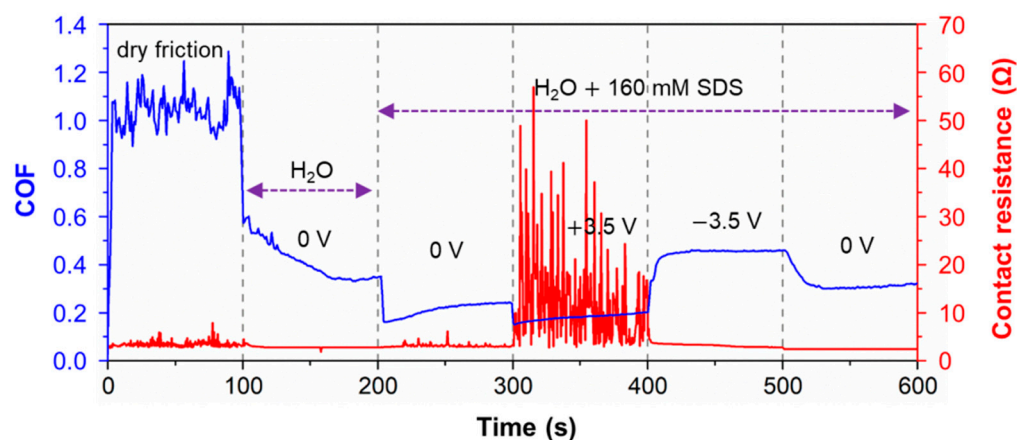


**Figure 3.** COF and contact resistance of the 316 L stainless steel plate and 304 stainless steel ball vs. time under different lubrication conditions (dry friction,  $H_2O$  lubrication, and 160 mM SDS aqueous solution lubrication) and different applied voltages ( $\pm 3.5$  V), with a reciprocating velocity of 8 mm/s and a load of 3 N under a pressure of 804 MPa.

Figure 4 shows the COF and contact resistance of Cu plate and 304 stainless steel ball verse time, under dry friction, pure PC lubrication, and 5 mM SDS PC solution lubrication. The COF under the dry friction was  $0.75 \pm 0.05$ , and the contact resistance was around  $1.3 \Omega$ . At 300 s, 0.25 mL pure PC was injected into the contact area. The COF decreased to  $0.52 \pm 0.03$  while the contact resistance remained almost constant. At 600 s, the COF further decreased to  $0.17 \pm 0.01$  when 20 mL SDS PC solution was added as a lubricant. While, the contact resistance was barely changed, around  $1.3 \Omega$ . When a positive potential of 20 V was applied on the surface of the lower friction pair, the COF decreased to 0.09, and the contact resistance obviously increased from  $1.3 \Omega$  to  $210.0 \Omega$  in 170 s. When a negative potential of 20 V was applied, the COF increased to 0.53. The contact resistance decreased to around

1.2  $\Omega$  under the negative potential or no applied potential, indicating the desorption of the SDS boundary film on the friction pair in the solution. The effect of the electric field on boundary lubrication was basically consistent, no matter whether H<sub>2</sub>O or PC was the base lubricant.

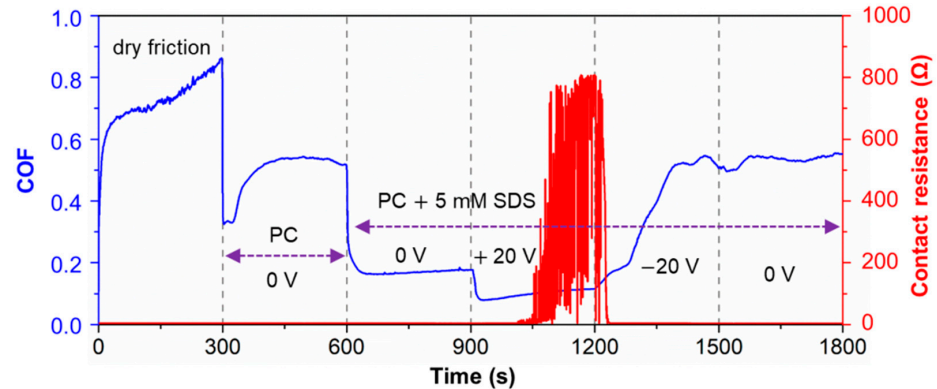


**Figure 4.** COF and contact resistance of the Cu plate and 304 stainless steel ball vs. time under different lubrication conditions (dry friction, pure PC lubrication, and 5 mM SDS PC solution lubrication) and different applied voltages ( $\pm 20$  V), with a reciprocating velocity of 8 mm/s and a load of 1 N under a pressure of 499 MPa.

### 3.2. On-Line Control of COF by Contact Resistance Detection and Applied Electric Field Control

Inspired by the friction results in Figures 3 and 4, a tribometer with an ECR module, an external electric field module, and an active control software design was designed to realize the on-line control of sliding friction of metals lubricated by adsorbed boundary SDS films.

Figure 5 shows the contact resistance and applied potentials during the friction test of the 316 L steel plate versus the 304 steel ball in 160 mM SDS aqueous solution. At the initial stage of the friction test, the contact resistance was relatively low because of the incomplete boundary film. After 9 s of an applied voltage of 3.5 V, the contact resistance increased from 2.3 to 8.5  $\Omega$ . At this stage, although the change of contact resistance was not significant, the COF decreased significantly. The related tribological results can be found in Figure 6, involving both the normal boundary lubrication without control and the one under control.

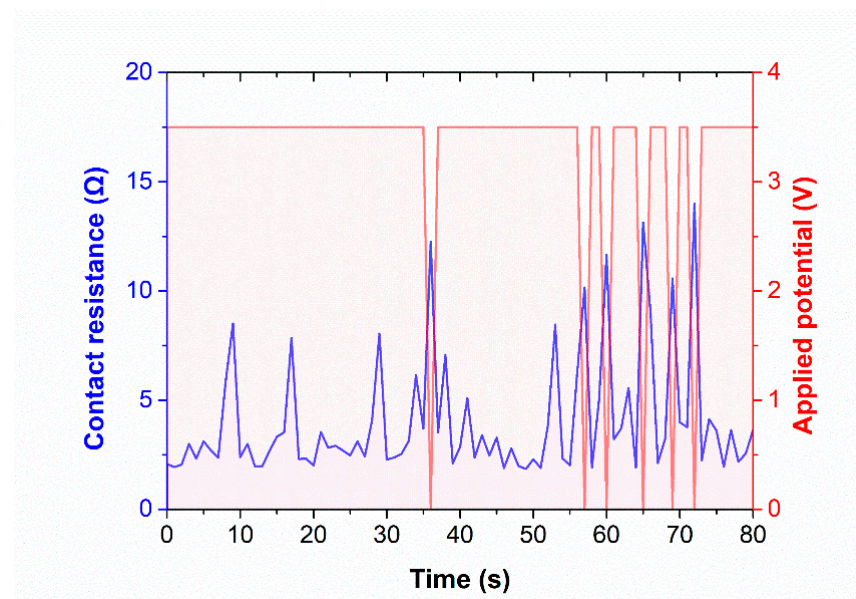


**Figure 5.** Contact resistance and applied potential vs. time during the friction test of 316 L steel plate vs. 304 steel ball in 160 mM SDS aqueous solution.

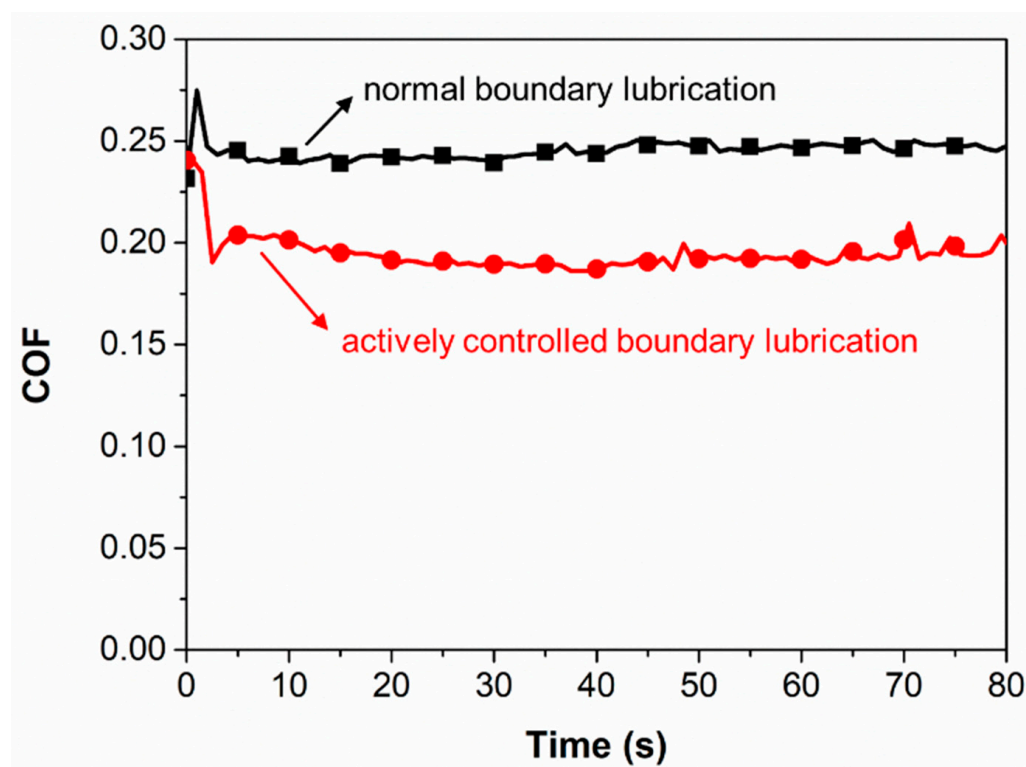


**Figure 6.** COF vs. time during friction tests for the normal boundary lubrication and the actively controlled boundary lubrication of 316 L steel plate vs. 304 steel ball in 160 mM SDS aqueous solution. For normal boundary lubrication without control, no applied potential was used; for actively controlled boundary lubrication, the applied voltage and the recorded contact resistance are shown in Figure 5.

When the contact resistance increased to  $12.2 \Omega$  (higher than the pre-set threshold of  $10.0 \Omega$ ) at 36 s, the power supply was switched off. The COF obtained under the actively controlled boundary lubrication in Figure 6 did not change significantly. Meanwhile, the contact resistance decreased obviously from  $12.2 \Omega$  to  $7.1 \Omega$ . The power supply was needed, so as to increase the contact resistance, and kept the COF at a good boundary lubrication state. After 36 s, the contact resistance was relatively high even in the absence of applied potentials, indicating that the boundary film state was relatively stable. This method ensures that the boundary lubrication film is in a good lubrication state while saving electric energy as much as possible. According to Figure 6, the COF was decreased by 24% (from 0.25 to 0.19), after the on-line control of the contact resistance of steel tribopairs in SDS aqueous solution by an external electric field. Compared to the case in which the external electric field was applied for the whole period of testing, the active controlling can save 7.4% of the electric energy in 80 s for the above friction system.

Figure 7a,b show the optical micrographs of the wear tracks of the 316 L steel plate after the friction tests as described in Figure 6. Figure 7c shows a comparison of the linear profiles, measured on the ZYGO profilometer (Middlefield, CT, USA), of these two wear tracks. For the normal boundary lubrication, the depth and length of the wear tracks were 0.42 and  $124.37 \mu\text{m}$ , respectively. For the actively controlled boundary lubrication, the depth of the wear tracks was around  $0.05 \mu\text{m}$ , and the width was around  $84.56 \mu\text{m}$ . The wear rate of the lower friction pair was reduced from  $4.56 \times 10^{-6} \text{ mm}^3/(\text{N}\cdot\text{m})$  to  $1.61 \times 10^{-6} \text{ mm}^3/(\text{N}\cdot\text{m})$ .

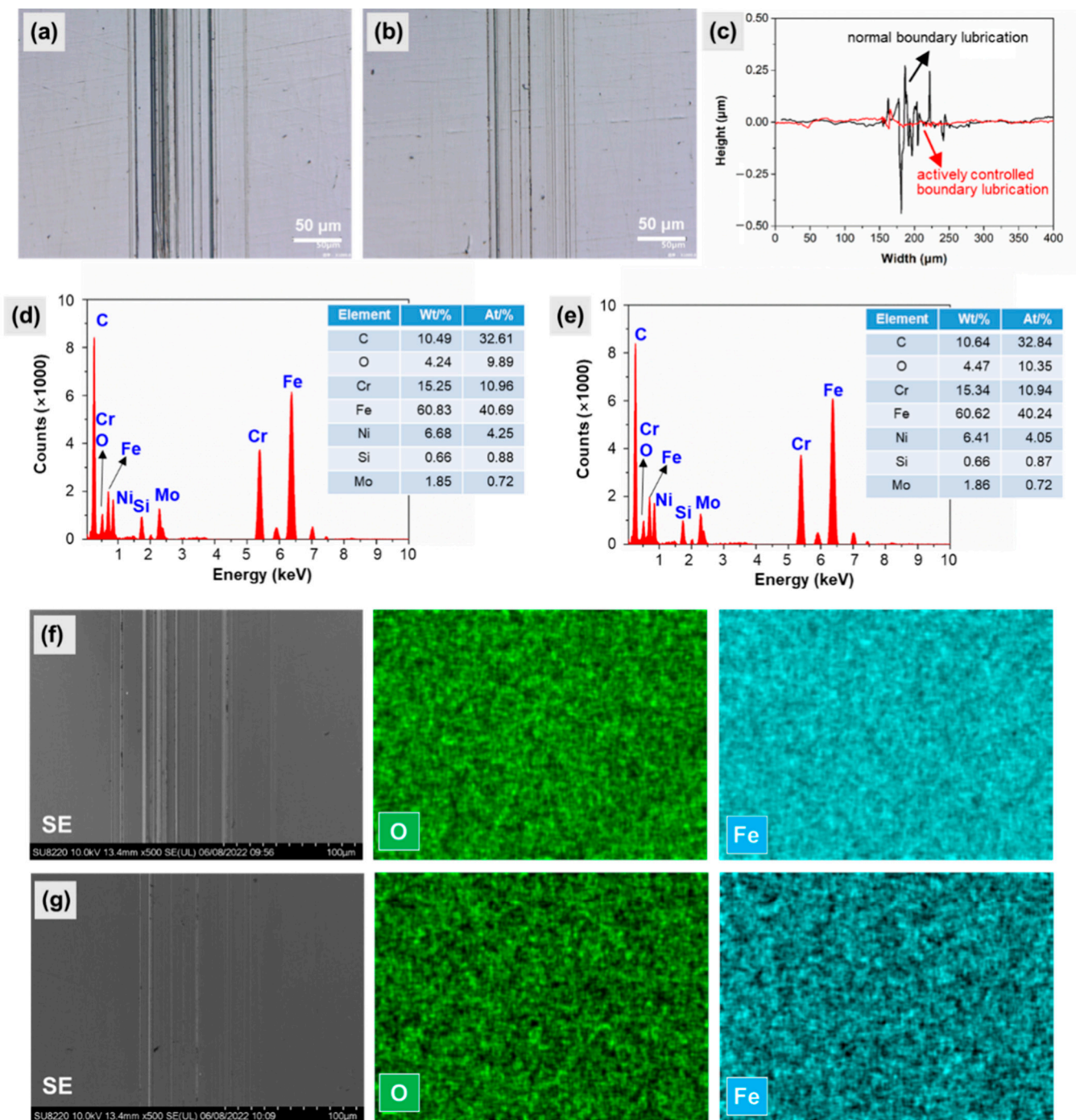


**Figure 7.** Characteristics of the wear tracks of the lower friction pairs obtained in the friction tests of 316 L steel plate vs. 304 steel ball in 160 mM SDS aqueous solution for 80 s: Optical micrographs of the wear tracks of the 316 L steel plate obtained in (a) the normal boundary lubrication and (b) the actively controlled boundary lubrication; (c) surface profiles of the wear tracks; element compositions of wear tracks of the 316 L steel plate obtained in (d) the normal boundary lubrication and (e) the actively controlled boundary lubrication; EDX elemental maps of the wear tracks of the 316 L steel plate obtained in (f) the normal boundary lubrication and (g) the actively controlled boundary lubrication.

Figure 7d reveals that the element compositions on the wear track of 316 L steel plate obtained in the normal boundary lubrication include C, O, Cr, Fe, Ni, Si, and Mo. The elements of Cr, Fe, Ni, Si, and Mo are the components of 316 L stainless steel. C and O are considered to come primarily from contaminants in the air or from lubricants. For

the element composition of the wear track obtained in the actively controlled boundary lubrication as shown in Figure 7e, the compositions and content of the elements are similar to those in Figure 7d. Furthermore, the surface morphologies and elemental maps of the wear tracks were inspected on SEM and EDX. Figure 7f,g respectively, show the results of the wear tracks obtained in the normal boundary lubrication and the actively controlled boundary lubrication. The green and blue areas in the figures represent the distributions of O and Fe elements, respectively. In both cases, the distribution of the O element inside and outside the wear tracks is consistent, indicating that no significant oxidation reactions occurred within the wear tracks. These results indicate that the external electric field can control the friction and wear behaviors by changing the adsorption film rather than the formation of the tribofilm or oxidation film on the friction pairs.

Figure 8 shows the COFs verse time for Cu plate/304 steel ball or Cu plate/bearing steel ball with 5 mM SDS PC solution as a lubricant before and after the active control. Here, we set the start time of active regulation as 0 s. As shown in Figure 8a, the COF obtained in the friction test of Cu plate/304 steel ball without active control (from  $-50$  s to 0 s) was  $0.18 \pm 0.01$ . After 0 s, it decreased to  $0.11 \pm 0.01$ . In Figure 8b, the COF decreased from  $0.28 \pm 0.01$  to  $0.13 \pm 0.01$ , after the on-line control of the contact resistance between Cu plate and bearing steel ball in SDS PC solution by an external electric field. The average COF was decreased by 39% for Cu plate/304 steel ball and 54% for Cu plate/bearing steel ball.

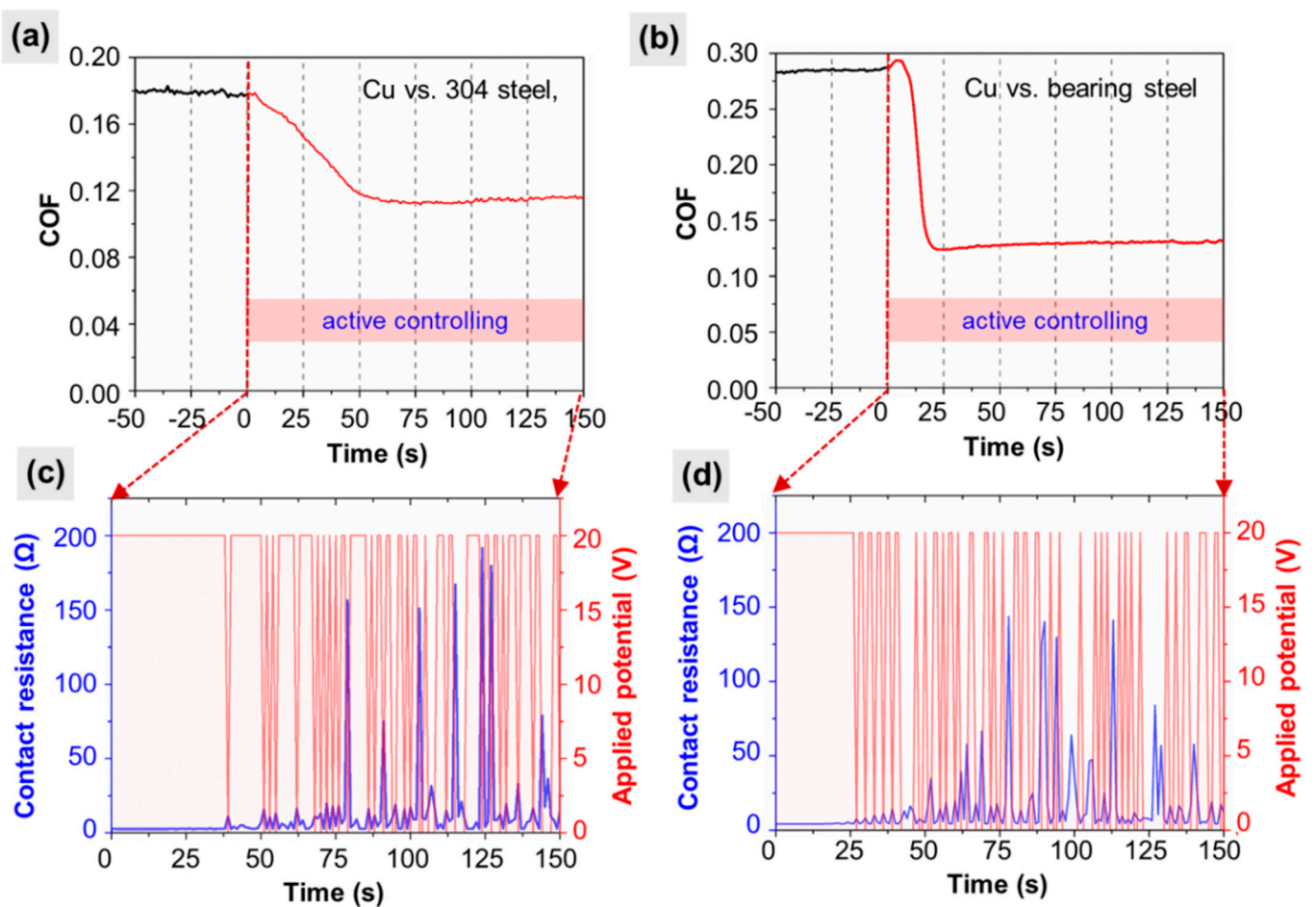


**Figure 8.** Effect of the actively controlled boundary lubrication in 5 mM SDS PC solutions. COF vs. time for (a) Cu plate/304 steel ball and (b) Cu plate/bearing steel ball; Contact resistance and applied potential vs. time for (c) Cu plate/304 steel ball, and (d) Cu plate/bearing steel ball.

According to the Hertzian contact model, the different hardness and Young's modulus of the two kinds of upper friction pairs cause the different Hertz pressures. Compared with the friction pair of Cu plate/304 steel ball, the relatively higher Hertz contact pressure for the friction pair of Cu plate/bearing steel ball causes a higher proportion of boundary film failure, resulting in the higher COF in the normal boundary lubrication condition. When a positive potential is applied, the adsorption capacity increases, and the adsorption strength of the boundary film becomes stronger, so as to achieve a better boundary lubrication effect. According to the adhesion friction theory, the COF is related to the shear strength of the boundary lubrication film and the yield stress of the soft material (pure Cu in this work). Hence, it can be considered that the COFs of the above two cases are similar under good SDS boundary lubrication (0.11 and 0.13). While, due to the different COFs during the normal boundary lubrication, the friction reductions after the actively controlled boundary lubrication are different.

Figure 8c,d show the contact resistance and applied potentials during the actively controlled boundary lubrication processes in Figure 8a,b, respectively. Similar to Figure 5, the contact resistances for the two cases were relatively low at the initial stage of the friction test. In Figure 8c, the contact resistance between the Cu plate and the 304 steel ball increased from 2.7  $\Omega$  to 11.1  $\Omega$  at around 39 s. Under the action of an electric field, the contact resistance gradually increased to around 190.0  $\Omega$ . The relatively high contact resistance indicates the formation of a good boundary lubrication film. In this case, the externally applied potential of 20 V was switched off when the contact resistance was higher than 10.0  $\Omega$ . The COF was stabilized at around 0.11, showing the preliminary realization of the smart lubrication and energy saving. For the case of the Cu plate and the bearing steel ball as friction pairs in Figure 8d, the contact resistance increased from 4.1  $\Omega$  to around 6.4  $\Omega$  and higher, after 25 s of an applied voltage of 20 V. In this case, the power supply was switched off, when the contact resistance reached 6.0  $\Omega$ . The contact resistance obtained under the actively controlled boundary lubrication increased to 177.5  $\Omega$ . After 50 s, the contact resistance was relatively high even in the absence of the potentials, indicating that the boundary film state was relatively stable. The active controlling can save about 25.8% and 49.7% of the electric energy for the Cu plate/304 steel ball and the Cu plate/bearing steel ball respectively, in 150 s.

Figure 9a,b show the optical micrographs of the wear tracks of the Cu plate obtained in normal boundary lubrication and actively controlled boundary lubrication of Cu plate vs. 304 steel ball in 5 mM SDS PC solution for 150 s. Figure 9c shows a comparison of the linear profiles between the two wear tracks described in Figure 9a,b. Compared with the normal boundary lubrication, the wear resistance is obviously improved in the actively controlled boundary lubrication for the Cu plate/304 steel ball pair in the SDS PC solution. The maximum depth of the wear track is reduced from 0.19 to 0.08  $\mu\text{m}$ . Figure 9d–f show the optical micrographs and linear profiles of the wear tracks of the Cu plate when rubbing against the bearing steel ball under the same as those in Figure 9a–c. The maximum depth of the wear track is reduced from 0.12 to 0.04  $\mu\text{m}$ . Combining with the results in Figures 8 and 9, we can conclude that the effect of voltages on the wear depth of cross-sections of wear tracks is consistent with that on COF.

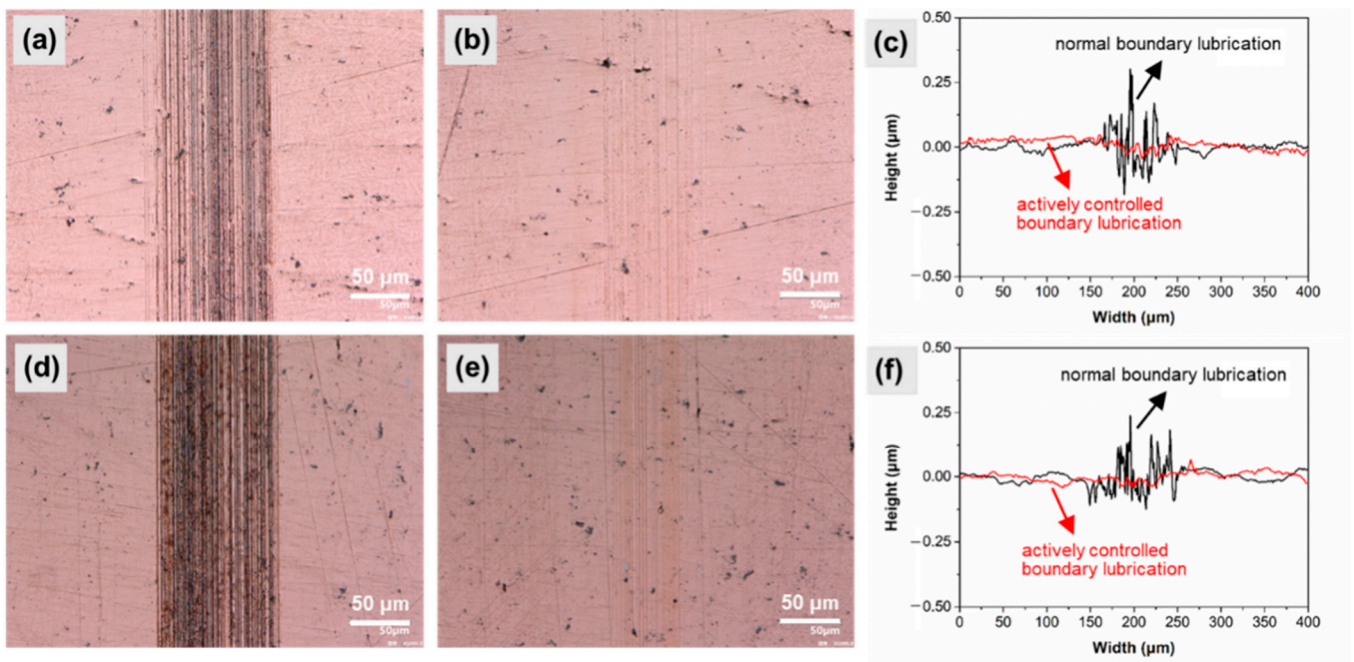


**Figure 9.** Characteristics of the wear tracks of the lower friction pairs obtained in the friction tests in 5 mM SDS PC solution for 150 s. Optical micrographs of the wear tracks of the Cu plate obtained in (a) the normal boundary lubrication and (b) the actively controlled boundary lubrication, and (c) the surface profiles of the wear tracks for Cu plate vs. 304 steel ball. Optical micrographs of the wear tracks of the Cu plate obtained in (d) the normal boundary lubrication and (e) the actively controlled boundary lubrication, and (f) the surface profiles of the wear tracks for Cu plate vs. bearing steel ball.

### 3.3. Discussions on Mechanism

The mechanism of achieving such an active regulation is summarized in the schematic diagram as shown in Figure 10. The contact area undergoes no boundary lubrication film, formation of boundary lubrication film, good boundary lubrication, and destruction of boundary lubrication film. No matter whether in water or PC oil, the addition of SDS can decrease the real contact area between the metals, resulting in an obvious decrease in COF. Nonetheless, the increase in contact resistance is not obvious due to some remaining local real contact areas. A relatively complete boundary film can be formed under certain positive potential, causing a significant increase in contact resistance. On the contrary, at the initial stage of boundary film failure, the change of contact resistance is quicker than that of COF. It is obvious that the combination of contact resistance and COF can provide more information on the working states of the boundary film between the metallic tribopairs, as contact resistance can reflect boundary film failure more quickly while COF can evaluate its formation more quickly. Hence, it is feasible to use contact resistance to characterize the state of boundary film and obtain relatively low COF.

To further discuss the effect of adsorption film on the COF and contact resistance during the boundary lubrication, dry friction tests were designed and carried out by excluding other effects such as tribochemical reactions or hydrodynamic lubrication. A clean 316 L stainless steel plate was soaked in a 10 mM SDS aqueous solution at room temperature. After 0.5 h, the steel plate was removed from the solution and dried at 100 °C for another 0.5 h. Figure 11a shows the schematic diagram of the experimental procedure. The COF and contact resistance of the treated sample and an untreated 304 stainless steel ball were tested on the UMT-3 and the auto ohmmeter.

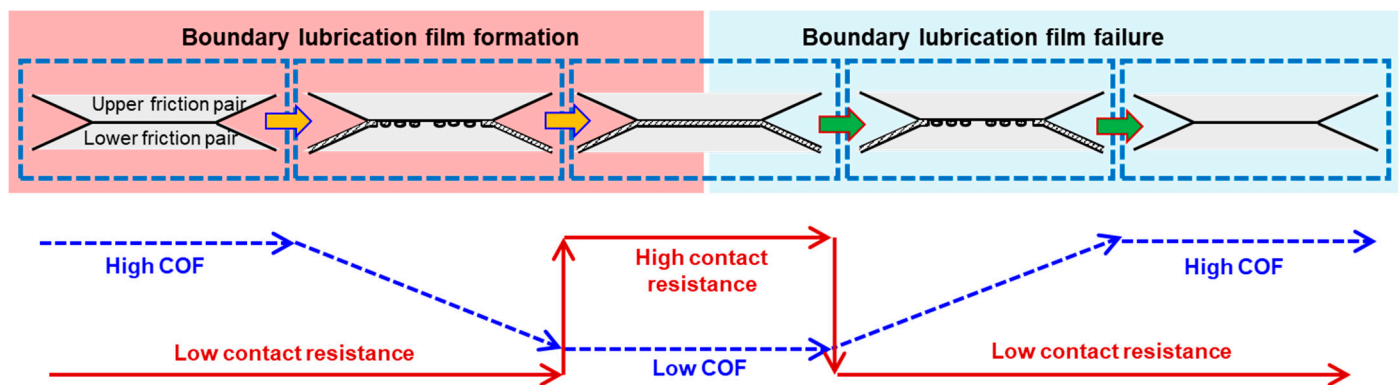


**Figure 10.** Schematic diagram of metallic asperity contacts undergoing no lubrication film, formation of boundary lubrication film, good boundary lubrication, and destruction of boundary lubrication film.

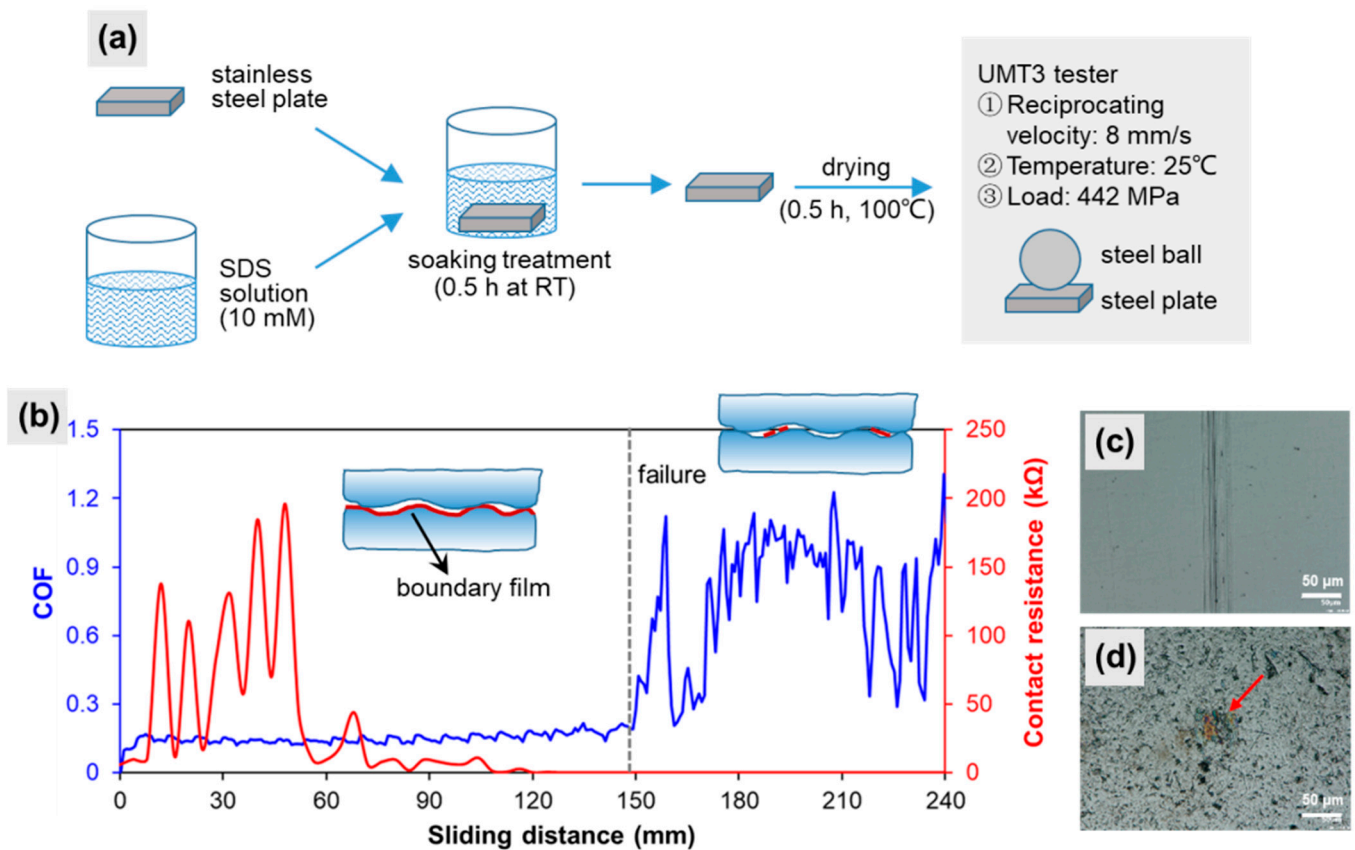


**Figure 11.** (a) Schematic diagram of the preparation and friction test of SDS adsorption film on stainless steel surface; (b) COF and contact resistance of the SDS treated 316 L steel plate and 304 stainless steel ball verse sliding distance under dry friction; (c) wear track of the lower friction pair and (d) wear spot on the upper friction pair after the friction test of 80 mm. The insets in (b) show the models of metallic asperity contacts before and after the failure of the boundary film.

Figure 11b shows the COF and contact resistance of the SDS treated 316 L steel plate and 304 stainless steel ball verse sliding distance during the dry friction. The friction tests were carried out with a reciprocating velocity of 8 mm/s under a pressure of 442 MPa. In the first 120 mm of the experiment, the COF was around 0.13 and the average contact resistance was around 39.3 k $\Omega$  (the maximum value reached 195.8 k $\Omega$ ). Figure 11c,d show the wear track of the lower friction pair and wear spot on the upper friction pair after the sliding distance of 80 mm (before the SDS boundary film was destroyed at ~150 mm).

The results show that under good boundary lubrication, abrasive particles were invisible around the friction pair. Compared with the contact resistance between 316 L steel plate and 304 steel ball in SDS aqueous solution, the contact resistance between the SDS treated 316 L steel plate and 304 steel ball in the air under its good boundary lubrication condition is much higher, which is considered to be caused by the adsorption film gradually transferred onto the top of the upper friction pair (as shown in Figure 11d) and the lack of solution conductivity. The contact resistance decreased from 10.8 k $\Omega$  to 1.4 k $\Omega$  at 105 m and further decreased to around 21  $\Omega$  at 128 m.

The increase of the COF before 150 m was not obvious. At around 150 m, the COF increased from 0.20 to 0.82. After the failure of the adsorbed film at 150 m, the average COF was around 0.71 and the average contact resistance was 6  $\Omega$ . These results reveal that the SDS adsorption film can decrease the COF and increase contact resistance. Moreover, the contact resistance is more sensitive to the failure of the boundary lubrication film, compared to the COF.

Contact resistance is generally composed of constriction resistance and film resistance [23,24]. Here, we discuss three cases as follows.

Peak contacts without covering film: Constriction resistance. The constriction resistance can be calculated from a solution of Laplace's equation using appropriate boundary conditions [28]. The electrical constriction resistance of one contact peak between the metallic tribopairs can be given as

$$R_c = \frac{\rho_1 + \rho_2}{4a} \quad (1)$$

where  $\rho_1$  and  $\rho_2$  is the electrical resistivity of the upper and lower friction pairs, and  $a$  is the constriction radius.

If the researched interface has a total of  $n$  contact peaks, the total contact resistance is  $\frac{1}{n}R_c$ .

All peak contacts covered with film: Film resistance. According to the definition of surface resistivity ( $\rho_s$ ) of films [29], the resistance encountered by electrons passing through a conductive film is given as

$$R_b = \frac{\rho_s}{\pi a^2} \quad (2)$$

Its total contact resistance  $R_j$  is the shunt resistance consisting of  $n$  series resistances of the constriction resistance and film resistance, as shown in Equation (3).

$$R_j = \frac{1}{n}R_c + \frac{1}{n}R_b = \frac{\rho_1 + \rho_2}{4na} + \frac{\rho_s}{\pi na^2} \quad (3)$$

Partially peak contacts are covered with film. Assume that the proportion of the number of contact peaks with boundary films is  $x$  of the total number of contact peaks. Then, the reciprocal of the total contact resistance is

$$\frac{1}{R} = \frac{(1-x)n}{R_c} + \frac{xn}{R_c + R_b} \quad (4)$$

therefore,

$$R = \frac{R_c}{n} \cdot \frac{R_c + R_b}{R_c + (1-x)R_b} \quad (5)$$

and

$$R = \frac{R_c}{n} \cdot \frac{1 + A}{1 + A - xA} \quad (6)$$

where  $A$  is equal to  $R_b/R_c$ .

The total contact resistance is related to  $x$  and  $A$ . When  $x$  is near 1, we can obtain that

$$R = \frac{R_c}{n} \cdot (1 + A) \quad (7)$$

According to the experimental result in Figure 11,  $R$  obtained under the good boundary lubrication is much larger than  $\frac{R_c}{\eta}$ , and  $A$  is around  $1 \times 10^3 \sim 30 \times 10^3$ . When  $0 < x < 1$ , it was obtained that the contact resistance was similar to that without boundary lubrication film ( $x = 0$ ). Therefore,  $xA \approx 0$ . These results indicate that once the boundary lubrication film starts to fail, the contact resistance will quickly drop in the absence of external voltage assistance.

#### 4. Conclusions

In this study, an on-line feedback control method of sliding friction of metallic tribo-pairs lubricated by adsorbed boundary SDS films has been realized by designing a customized tribometer with an ECR module, an external electric field module, and an active control software design. The contact resistance, combined with the COF, can provide more information on the working states of the adsorbed boundary films. It is feasible to use contact resistance to characterize the state of boundary film and obtain the relative low COF, as contact resistance can reflect boundary film failure more quickly while COF can evaluate its formation more quickly.

When a positive voltage was applied, the adsorption of SDS anions on the surface of the friction pair was enhanced so that the boundary film was in a stable state. When the contact resistance increased to a pre-set threshold (e.g., 6~10  $\Omega$ ), the external voltage was switched off. It ensures that the boundary lubrication film is in a good lubrication state while saving electric energy as much as possible. For the 160 mM SDS aqueous solution as a lubricant, the COF decreased from 0.25 to 0.19 for 316 L steel plate/304 steel ball with an applied potential of + 3.5 V. For the 5 mM SDS PC solution as a lubricant, the average COF decreased from 0.18 to 0.11 for Cu plate/304 steel ball and from 0.28 to 0.13 for Cu plate/bearing steel ball with an applied potential of + 20 V. It is expected to provide a new pathway for the development of next-generation smart tribological systems.

**Author Contributions:** Conceptualization, Y.M.; experimentation, C.L., X.L. (Xiaosong Li) and X.L. (Xinxin Li); software, X.L. (Xiaosong Li); validation, C.L. and X.L. (Xiaosong Li); formal analysis, C.L.; writing—original draft preparation, C.L., X.L. (Xiaosong Li) and X.L. (Xinxin Li); writing—review and editing, Y.M.; project administration, Y.M, Y.T. and W.L. All authors have read and agreed to the published version of the manuscript.

**Funding:** This research was funded by the National Natural Science Foundation of China (Grant No. 51961145303, Grant No. 5191101008, Grant No. 5210050195), China Postdoctoral Science Foundation (Grant No. 2021TQ0175) and Tsinghua (SVM)-Shell Joint Research Center for Clean Mobility under the Work Order No. CW 299060.

**Institutional Review Board Statement:** Not applicable.

**Informed Consent Statement:** Not applicable.

**Data Availability Statement:** For more detailed data, please request from the corresponding author or the first author.

**Conflicts of Interest:** The authors declare no conflict of interest.

#### References

1. Wen, S.; Huang, P. *Principles of Tribology*, 2nd ed.; Tsinghua University Press: Beijing, China, 2017.
2. Glavatskih, S.; Höglund, E. Tribotronics—Towards active tribology. *Tribol. Int.* **2008**, *41*, 934–939. [[CrossRef](#)]
3. He, F.; Xie, G.; Luo, J. Electrical bearing failures in electric vehicles. *Friction* **2020**, *8*, 4–28. [[CrossRef](#)]
4. Taylor, R.I. Energy efficiency, emissions, tribological challenges and fluid requirements of electrified passenger car vehicles. *Lubricants* **2021**, *9*, 66. [[CrossRef](#)]
5. Krim, J. Controlling friction with external electric or magnetic fields: 25 examples. *Front. Mech. Eng.* **2019**, *5*, 22. [[CrossRef](#)]
6. Bowden, P.F.; Young, L. Influence of interfacial potential on friction and surface damage. *Research* **1950**, *3*, 235–237.
7. Bockris, J.O.; Argade, S.D. Dependence of friction at wet contacts upon interfacial potential. *J. Chem. Phys.* **1969**, *50*, 1622–1623. [[CrossRef](#)]
8. Wang, S.S.; Maheswari, S.P.; Tung, S.C. The nature of electrochemical reactions between several zinc organodithiophosphate antiwear additives and cast iron surfaces. *Tribol. Trans.* **1989**, *32*, 91–99. [[CrossRef](#)]

9. Tung, S.C.; Wang, S.S. In-situ electro-charging for friction reduction and wear resistant film formation. *Tribol. Trans.* **1991**, *34*, 479–488. [[CrossRef](#)]
10. Zhu, Y.Y.; Kelsall, G.H.; Spikes, H.A. The influence of electrochemical potentials on the friction and wear of iron and iron oxides in aqueous systems. *Tribol. Trans.* **1994**, *37*, 811–819. [[CrossRef](#)]
11. He, S.; Meng, Y.; Tian, Y.; Zuo, Y. Response characteristics of the potential-controlled friction of zro2/stainless steel tribopairs in sodium dodecyl sulfate aqueous solutions. *Tribol. Lett.* **2010**, *38*, 169–178. [[CrossRef](#)]
12. Yang, X.; Meng, Y.; Tian, Y. Effect of imidazolium ionic liquid additives on lubrication performance of propylene carbonate under different electrical potentials. *Tribol. Lett.* **2014**, *56*, 161–169. [[CrossRef](#)]
13. Yang, X.; Meng, Y.; Tian, Y. Potential-controlled boundary lubrication of stainless steels in non-aqueous sodium dodecyl sulfate solutions. *Tribol. Lett.* **2014**, *53*, 17–26. [[CrossRef](#)]
14. Liu, C.; Friedman, O.; Meng, Y.; Tian, Y.; Golan, Y. Cus nanoparticle additives for enhanced ester lubricant performance. *ACS Appl. Nano Mater.* **2018**, *1*, 7060–7065. [[CrossRef](#)]
15. Meng, Y.; Jiang, H.; Wong, P.L. An Experimental Study on Voltage-Controlled Friction of Alumina/Brass Couples in Zinc Stearate/Water Suspension. *Tribol. Trans.* **2001**, *44*, 567–574. [[CrossRef](#)]
16. Gatti, F.; Amann, T.; Kailer, A.; Baltés, N.; RuChe, J.; Gumbsch, P. Towards programmable friction: Control of lubrication with ionic liquid mixtures by au-tomated electrical regulation. *Sci. Rep.* **2020**, *10*, 17634. [[CrossRef](#)]
17. Yamaguchi, E.S.; Roby, S.H.; Ryason, P.R.; Yeh, S.W. Electrical contact resistance bench wear testing: Comparison with engine test results. In *SAE Powertrain & Fluid Systems Conference & Exhibition*; SAE International: Warrendale, PA, USA, 2002.
18. Tian, P.; Tian, Y.; Shan, L.; Meng, Y.; Zhang, X. A correlation analysis method for analyzing tribological states using acoustic emission, frictional coefficient, and contact resistance signals. *Friction* **2015**, *3*, 36–46. [[CrossRef](#)]
19. Rossing, T.D. *Handbook of Acoustics*; Springer: Berlin/Heidelberg, Germany, 2014.
20. Archard, J.F. Contact and rubbing of flat surfaces. *J. Appl. Phys.* **1953**, *24*, 981–988. [[CrossRef](#)]
21. Greenwood, J.A. Constriction resistance and the real area of contact. *Br. J. Appl. Phys.* **1966**, *17*, 1621–1632. [[CrossRef](#)]
22. Holm, R. *Electric Contacts Handbook*; Springer: Berlin/Göttingen/Heidelberg, Germany, 1958.
23. Wei, P.S.; Wu, T.H. Electrical contact resistance effect on resistance spot welding. *Int. J. Heat Mass Transf.* **2012**, *55*, 3316–3324. [[CrossRef](#)]
24. Zhang, P.; Lau, Y.Y. Constriction resistance and current crowding in vertical thin film contact. *IEEE J. Electron. Devices Soc.* **2013**, *1*, 83–90. [[CrossRef](#)]
25. Ji, H.; Nicholls, M.A.; Norton, P.R.; Kasrai, M.; Capehart, T.W.; Perry, T.A.; Cheng, Y. Zinc-dialkyl-dithiophosphate antiwear films: Dependence on contact pressure and sliding speed. *Wear* **2005**, *258*, 789–799. [[CrossRef](#)]
26. Bai, L.; Meng, Y.; Zhang, V.; Khan, Z.A. Effect of surface topography on zddp tribofilm formation during running-in stage subject to boundary lubrication. *Tribol. Lett.* **2022**, *70*, 10. [[CrossRef](#)]
27. Meng, Y.; Liu, C. Spatiotemporal manipulation of boundary lubrication by electro-charging and electrochemical methods. In *Superlubricity*, 2nd ed.; Erdemir, A., Martin, J.M., Luo, J., Eds.; Elsevier: Amsterdam, The Netherlands, 2021; pp. 499–516.
28. Timsit, R.S. Electrical contact resistance: Properties of stationary interfaces. *IEEE Trans. Compon. Packag. Technol.* **1999**, *22*, 1–19. [[CrossRef](#)]
29. Boyer, L. Contact resistance calculations: Generalizations of greenwood's formula including interface films. *EEE Trans. Compon. Packag. Technol.* **2001**, *24*, 50–58. [[CrossRef](#)]